Journal of Energy Storage 72 (2023) 108315

Contents lists available at ScienceDirect

Journal of Energy Storage

journal homepage: www.elsevier.com/locate/est

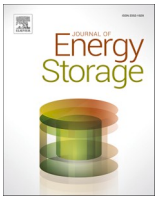

Research papers

Investigation of propagation of thermal runaway during large-scale storage and transportation of Li-ion batteries

Dhananjay Mishra [a,1], Raghavender Tummala [b], Ankur Jain [a,*]

[a] Mechanical and Aerospace Engineering Department, University of Texas at Arlington, Arlington, TX, USA
[b] Electric Vehicle Occupational Safety (EVOS), General Motors Company, Warren, MI, USA

ARTICLE INFO

Keywords:
Thermal runaway
Li-ion batteries
Battery safety

ABSTRACT

Thermal runaway in Li-ion cells and battery packs impacts the safety and performance of electrochemical energy storage systems. In particular, preventing the propagation of thermal runaway in large-scale battery storage and transportation of batteries is of much importance. While most of the past work in this direction addresses single cells or a small battery pack, only limited literature is available on systems of larger size. This work presents multiphysics simulations of propagation of thermal runaway during large-scale storage and transportation of Li-ion cells. Through simulations that account for multimode heat transfer, Arrhenius heat generation, turbulent fluid flow and combustion, the propagation of thermal runaway from one pallet of cells to an adjacent pallet is studied. The model quantitatively predicts the temperature field in/around the pallets, and, in particular, predicts whether the adjacent pallet will also catch fire or not. The impact of state of charge of the cells on thermal runaway propagation is examined. Results indicate that the gap between pallets plays a key role in determining propagation. A sharp threshold value of the gap is found, beyond which, propagation does not occur. Results from this work may be helpful in ensuring thermal safety during large-scale storage and transportation of Li-ion cells, ultimately contributing towards improved electrochemical energy storage and conversion.

1. Introduction

Li-ion cells are used commonly for electrochemical energy conversion and storage in automobiles [1], spacecraft [2], renewable grid energy storage [3] and consumer electronics. Li-ion cells offer excellent energy storage characteristics, including high energy storage density, excellent cyclability, low self-discharge rate and minimal memory effect. However, Li-ion cells are known to be very temperature-sensitive, with rapid deterioration in performance at low or high temperatures [4]. In addition, overheating of a Li-ion cell also presents the risk of thermal runaway, which refers to a series of sustained decomposition reactions that are triggered at a high temperature and usually lead to fire and explosion [5]. These reactions, including decomposition of the electrode materials, binders, separator and the electrolyte have strongly temperature-dependent reaction rates, which sets up positive feedback between temperature rise and heat generation. The prediction [6] and prevention [7,8] of thermal runaway remains a key challenge in Li-ion battery safety.

Due to its critical importance in battery safety, thermal runaway has been studied in detail through both measurements and modeling. The key decomposition reactions that occur during thermal runaway onset have been experimentally characterized [9], and well-known reaction models have been proposed. Due to the hazards and cost associated with experimental measurements, theoretical models have been heavily used to predict the nature of thermal runaway and to guide the design of thermal runaway experiments. Within a single cell, temperature-dependent heat generation models containing a single reaction [10,11] or multiple reactions [9,12] are often used along with anisotropic thermal transport properties [13]. Lumped [14,15] as well as one- [16] or multi-dimensional [17,18] models have been used to characterize thermal runaway in a single cell. It is well-known that the state-of-charge (SoC) of the cell plays a key role in determining its thermal runaway characteristics. For most cell chemistries, cells at higher SoC exhibit severe and more catastrophic response to abuse scenarios as compared to cells at lower SoC [19]. Increase in SoC increases the number and energy of gases vented during thermal runaway onset and propagation [20], resulting in greater amount of energy released and increased thermal runaway hazard [21]. Typically, cells are shipped at

* Corresponding author at: 500 W First St, Rm 211, Arlington, TX 76019, USA.
E-mail address: jaina@uta.edu (A. Jain).
[1] Present Affiliation: Electric Vehicle Occupational Safety (EVOS), General Motors Company, Warren, MI, USA.

https://doi.org/10.1016/j.est.2023.108315
Received 21 March 2023; Received in revised form 21 May 2023; Accepted 6 July 2023

relatively low SoCs of around 25–30%.

In the context of a battery pack comprising multiple cells, the propagation of thermal runaway from one cell to its neighbors is an important problem because such propagation can completely destroy the entire pack. Propagation of thermal runaway may occur due to multiple non-linear and often highly coupled transport processes, including thermal conduction through the interstitial material [18], radiation heat transfer [22], thermal advection due to hot venting gases from a ruptured cell [23] and combustion of volatile gases ejecting from the cell [24]. Accordingly, some of the key aspects that determine whether propagation occurs or not include the rupture location, whether the vent gases catch fire [24], the nature of interstitial material, including the material of the partition sleeves commonly used for packing cells [22] and the cell-to-cell gap in the battery pack [25]. The impact of each of these aspects on thermal runaway propagation has been studied in the past. Several aspects of the underlying transport processes make the modeling of thermal runaway propagation in a battery pack a computationally challenging task. For example, around the onset of thermal runaway, the extremely large heat release rate and temperature rise requires very small time steps, which significantly slows down simulations. Further, high speed – often supersonic – turbulent flow of vent gases [26], combustion of multiple vent gases [24] and radiation [22] – each of which are non-linear by themselves – when combined, result in a very expensive computational problem. Therefore, the number of cells considered in such simulations is often limited to only a few, whereas practical battery packs often contain thousands of cells, and the number of cells during storage and transportation may be even greater. Optimizing and reducing the computational burden remains an important challenge [27] in order to develop simulations that can be conveniently used as design tools.

While the literature cited above covers thermal runaway in a single cell and propagation within a small pack of cells, there is only limited literature available on very large Electric Vehicle (EV) modules or pallets containing a large number of cells during storage and transportation. Rigorous fire test methods [28] have identified a direct relationship between state of charge of the cell and catastrophic fire behavior in such scenarios. Studies have shown that the maximum value for heat of combustion can be as high as 18 MJ with heat release rate as high as 49.4 kW [29]. As a result, steps to retard fire propagation are largely implemented at both small scale by adding flame retardant additives [30], separators [31] and at large scale by implementing fire suppression mechanisms in large storage/transportation facilities [32,33]. Simulation models involving fire onset and propagation are computationally expensive [34]. A recent work has presented simulation of thermal runaway related fire in a battery storage facility [33]. However, the modeling of chemical kinetics related to thermal runaway was empirical rather than physics-based in this work, thereby limiting its applicability for studying other battery fire scenarios. While the submodeling technique has been used for studying thermal management of a pack containing thousands of cells [35], this technique is limited only to linear processes and will not work well in modeling non-linear thermal runaway. Despite these challenges, there is clearly a need for understanding the large-scale propagation of thermal runaway and fire in energy storage systems. In doing so, it may be necessary to sacrifice small-scale details, such as the length scale of electrodes within each cell, or even cells themselves in order to execute such simulations within a reasonable time. Such simulations may contribute towards ensuring the safety of storage and transportation processes.

This work presents a numerical simulations based investigation of thermal runaway propagation during large-scale storage or transportation of Li-ion batteries. The model captures thermal runaway onset and fire due to combustion of vent gases, and predicts the transient temperature field in close proximity of pallets containing a large number of cells. The model is used to understand the role of SoC and geometrical parameters that affect thermal runaway propagation.

2. Simulation model

2.1. Geometry and general modeling framework

Fig. 1(a) shows a schematic of the simulation geometry that comprises two pallets of 18650 Li-ion cells kept next to each other in a large storage facility. Each pallet contains one hundred 18650 NCA Li-ion cells arranged in a 10 × 10 array. The goal of the simulations is to understand the outcome of thermal abuse of one of the pallets, referred to as the trigger pallet. Specifically, it is of interest to determine the resulting temperature field in the storage facility and predict whether propagation of thermal runaway and fire to the adjacent pallet occurs or not.

There are several computational challenges associated with such a simulation. Firstly, the length scales in this problem range across multiple orders, from the thin electrode layers within each layer that generate heat to the length scale of the storage facility itself. This multiscale nature of the problem makes it computationally very expensive to model the fine geometrical details while also modeling larger length scales. To address this, the geometrical details of each cell with a pallet are ignored and each pallet is assumed to have homogeneous thermal properties, corresponding to those of individual cells. Crucially, temperature-dependent heat generation due to decomposition reactions in the cells that is ultimately responsible for thermal runaway is preserved in its original form within each pallet, and so is the anisotropic thermal conduction within the pallet. While this homogenization of the pallet may introduce some computational errors, if executed properly, it offers a reasonable compromise between accuracy and computational cost, as evidenced by its use in several past papers on computational modeling of large multiscale systems [35,36].

Further complications arise in this problem from the several non-linear phenomena relevant to this problem that are also highly coupled with each other. These include combustion, turbulent flow, and radiative heat transfer. Details of the physics models for these processes are discussed in subsequent sub-sections. Key computational and meshing details are also outlined.

2.2. Governing equations

2.2.1. Abuse model and vent gas generation

The four-equation thermal abuse model for a Li-ion cell presented by Kim, et al. [9], which has been empirically represented by a one-step reaction model by Kim, et al. [11] is used in this work. The rate of reaction is defined by

$$\frac{d\alpha}{dt} = -A\cdot\alpha^{m}\cdot(1-\alpha)^{n}\cdot\exp\left(\frac{-E_a}{RT}\right)\cdot\exp(-B\cdot\alpha) \quad (1)$$

where A is the frequency factor, E_a is the activation energy, R is the universal gas constant and m, n and B are predefined reaction constants. α is the degree of progress of the reaction [9]. The values of abuse reaction parameters corresponding to NCA 18650 cells at 25% SOC [11] are used in this work and are tabulated in Table 1. Following Eq. (1), the source term for the energy equation is given by

$$\dot{Q}''' = H\cdot\frac{d\alpha}{dt} \quad (2)$$

where H is the specific heat release.

The initial temperature of trigger pallet is taken to be 500 °C, which initiates the decomposition reactions. This is representative of a general abuse scenario, and is a reasonable simplification since the focus of the work is to study phenomena during thermal runaway rather than the abuse scenarios leading to thermal runaway. As time passes, the adjacent pallet experiences thermal abuse by virtue of heat released due to combustion of vent gases from the trigger pallet.

It is assumed that gases are generated in proportion to the rate of

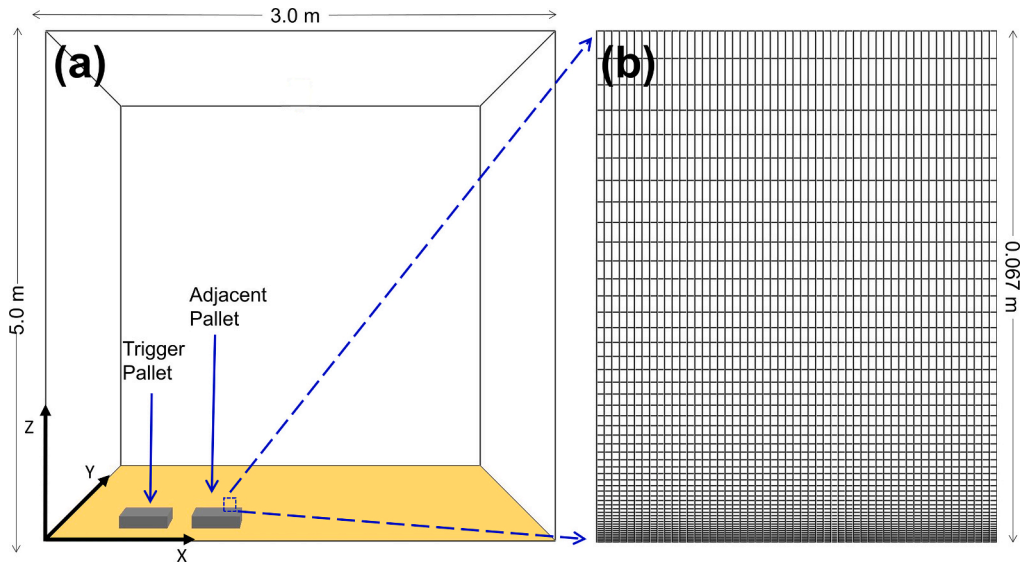

Fig. 1. Schematic of two 0.184 m × 0.184 m × 0.069 m pallets containing 18650 Li-ion battery packs kept in a storage facility showing overall simulation geometry showing the trigger and adjacent pallet. (b) Computational mesh in the XZ plane close to the top of the pallets.

Table 1
Values of abuse parameters used for single step abuse model [11].

Abuse Parameters	Values		
	25% SoC	50% SoC	100% SoC
H (kJ m^{-3})	1.55×10^6	1.98×10^6	1.96×10^6
A (s^{-1})	3.5×10^{18}	7.77×10^{18}	5.76×10^{18}
E_a (kJ $kmol^{-1}$)	1.90×10^5	1.92×10^5	1.83×10^5
m	0	0	0
n	0.25	0.25	0.25
B	24	26	27.5

abuse reaction. Equations governing the generation of gases from the pallet are given by

$$M_{cell} = x \cdot M_{gas} + (1 - x) \cdot M_{residue} \tag{3}$$

$$\frac{dM_{gen,total}}{dt} = x \cdot W \cdot \frac{d\alpha}{dt} \tag{4}$$

$$\frac{dM_{gen,species}}{dt} = Y_{species} \cdot M_{gen,total} \tag{5}$$

where x is the mass fraction of the cell changing to gas and W is the active material content. M_{gas} is the mass of gases generated during combustion which plays a crucial role in total heat release calculation using Eq. (3). $Y_{species}$ refers to the experimentally determined mass fraction. These volatile gases ignite once ignition temperature is reached. Once the gases are generated, isotropic diffusion model given by Fick's law governs the diffusion of gases into the free stream. Depending on simulation conditions, the heat sinking effect of the adjacent pallet may be overwhelmed by the thermal runaway heat generation in the trigger pallet. Based on past work, gaseous species involved in the combustion are taken to be H_2, CO_2, CO, CH_4, C_2H_4 and C_2H_6 respectively [5]. Mean mass fractions for these species for NCA type 18650 Li-ion cell are widely available [11]. Also, based on past experimental work, it is assumed that 1% of the total cell mass converts to soot [37]. Total mass of a single 18650 cell is taken to be 45 g.

Boundary surfaces of the simulation geometry are open to atmosphere, except the floor, in order to realistically capture combustion in a large storage facility. Open boundaries allow flow of gases and heat out of the simulation domain. Additionally, it is assumed that there is no forced ventilation.

2.2.2. Impact of SoC

Since the SoC of the cell determines its energy content, therefore, the SoC is likely to play a key role in determining its thermal runaway characteristics. Total heat release, total mass loss and the severity of ejection all increase with increasing SoC [20]. These adverse characteristics make the cell more vulnerable to external abuse conditions and increase the probability of cascade and fire propagation [21]. Increase in SoC increases the availability of lithium in the anode, which reacts with electrolytes after SEI decomposition to generate flammable gases. This further leads to increase in combustion-generated heat, thus increasing the severity of combustion. Arrhenius kinetic parameters for different SoCs are determined from curve-fitting experimental data [38] and are described in detail in past work [11].

2.2.3. Governing equations in the free stream

Large Eddy Simulation (LES) turbulence model [39] is used in these simulations to model buoyant fumes and low Mach number flow of species undergoing combustion. This model significantly reduces computational cost of the simulation due to direct computation of large-scale motion in the flow. Conservation of mass in the flow field, species conservation in the flow field, variation of momentum and conservation of energy in the free stream are modeled as follows

$$\frac{\partial \rho}{\partial t} + \nabla \cdot (\rho \cdot V) = \frac{dm'''}{dt} \tag{6}$$

$$\frac{\partial (\rho \cdot Y_{species})}{dt} + \nabla \cdot (\rho \cdot Y_{species} \cdot V) = \nabla (\rho \cdot D_{species} \cdot \nabla \cdot Y_{species}) + \frac{dM_{chem}}{dt} + \frac{dM_{evap}}{dt} \tag{7}$$

$$\frac{\partial (\rho \cdot V)}{dt} + \nabla \cdot (\rho \cdot V \cdot V) = -\nabla P_{pr} - \nabla \tau + (\rho - \rho_o) g + S_p + S_{evap} \tag{8}$$

$$\frac{\partial (\rho \cdot h_s)}{\partial t} + \nabla \cdot (\rho \cdot h_s \cdot V) = \frac{DP}{Dt} + \frac{dQ'''_{release}}{dt} - \nabla \cdot Q'''_{flow} \tag{9}$$

Description of key variables appearing in equations above is provided in Table 2. Eqs. (6) and (7) denote mass and species conservation within the flow field. In the given simulation set up, generation of a particular species may occur due to chemical reactions and combustion following thermal runaway, or due to evaporation of a liquid. Both of these processes are accounted for in Eq. (7). Eq. (8) represents conservation of momentum within the flow field. The right hand side of this

Table 2
List of variables appearing in turbulence transport equations.

Variable	Description
m'''	Mass generation per unit volume
$Y_{species}$	Mean mass fraction of the species
ρ	Density
V	Velocity vector
$D_{species}$	Diffusion coefficient of species
M_{chem}	Mass generation per unit volume of a species by chemical reaction
ρ_o	Initial density
τ	SGS stress tensor
h_s	Sensible enthalpy
P_{pr}	Pressure perturbation
$Q'''_{release}$	Heat release per unit volume
S_p	Momentum transfer due to particles
S_{evap}	Momentum transfer due to evaporation
Q''_{flow}	Heat flux vector

equation contains terms such as change in pressure perturbation, change in momentum due to buoyant flow, change in momentum due to soot particles and change in momentum due to evaporation. For low Mach number flows, internal energy and enthalpy of the flow can be related to thermodynamic pressure. Therefore, in terms of sensible enthalpy, conservative energy equation for the flow field is written in the form shown in Eq. (9).

2.2.4. Thermal transport mechanisms

Three key modes of thermal transport between pallets – conduction, natural convection and radiation – are accounted for in the energy equation given by Eq. (9). The treatment of these mechanisms is similar to past work on thermal runaway propagation in smaller battery packs [18]. Briefly, conduction is modeled through the standard Fourier equation, both within each pallet and in the air between pallets. Anisotropic thermal conductivity of the pallet is specified for this purpose, so that the temperature field within each pallet is governed by the following equation:

$$k_x\frac{\partial^2 T}{\partial x^2}+k_y\frac{\partial^2 T}{\partial y^2}+k_z\frac{\partial^2 T}{\partial z^2}+Q'''=\rho c_p\frac{\partial T}{\partial t} \tag{10}$$

Due to large size of simulation domain and computational constraints, specific details of each material inside a cell are not modeled. Each pallet is considered to have homogeneous thermal properties. These assumptions are necessary due to the large scale of the overall geometry. This is also reasonable because the interest here is in studying the temperature field and propagation outside the pallet. Natural convection in the surrounding air is modeled using the Boussinesq approximation. Radiative heat transfer is modeled using a surface-to-surface radiative model, for which, view factors are calculated using the ray tracing method. Details of these models are available in recent past work [18].

2.2.5. Finite rate combustion

A mixing-controlled combustion model with infinite reaction rate is used to model heat generation during combustion, including consumption of reactants during thermal runaway onset and propagation. In order to accurately model change in concentration of volatile species, the rate of combustion is considered to be a function of both temperature and concentration. A finite-rate Arrhenius kinetics based single-step reaction model is used. Reaction parameters for finite rate combustion of various species are taken from past work [11] as summarized in Table 3. Equations defining single step combustion are as follows:

$$\frac{dC_s}{dt}=-k_s\prod C_s^{N_s'} \tag{11}$$

$$k_s=A_s\cdot T^p\cdot e^{-E_{a,s}/RT} \tag{12}$$

Table 3
Values of Arrhenius parameters for gaseous components used in combustion model [11].

Species	Pre-exponential factor (mol cm^{-3} s^{-1})	Activation energy (kJ mol^{-1})
H_2	1.91×10^{14}	71.4
CH_4	1.3×10^{8}	48.4
CO	4.4×10^{6}	199.4
C_2H_4	2×10^{12}	30
C_2H_6	4.2×10^{11}	38.8

where s refers to a species and the product in Eq. (10) is carried out over all reactions. Values of N_s and p are taken to be 1 and 0, respectively [40].

2.3. Meshing and other simulation details

All simulations are carried out in Fire Dynamics Simulator (FDS) [41], which has been used in several past papers related to combustion and fire propagation [42–44]. Graphival visualization of simulation results is carried out in Smokeview (SMV) software. Simulations involving buoyant fumes and fires usually require extremely fine discretization to achieve reasonable accuracy. In the present work, a non-uniform mesh resolution is used with 0.0015 m as the largest element size to manage computational time. Non uniformity is modeled in z direction using piecewise linear mesh transformation technique. As a result, mesh resolution is maximum in the vicinity of the pallet and reduces with height. Higher resolution results in greater number of elements covering the characteristic fire length, which, in turn enhances numerical stability. A picture of the computational mesh in the XZ plane close to the top of the pallets is shown in Fig. 1(b).

Adaptive time stepping is used throughout. The largest timestep is restricted to 10 ms in order to keep the Courant-Friedrichs-Lewy (CFL) [45] and von Neumann [46] stability constants below 0.7 to ensure stability.

3. Results and discussion

3.1. Grid- and timestep-independence of simulation results

Due to the highly non-linear nature of various processes associated with thermal runaway propagation that are being accounted for in the simulation model, it is important to first establish the accuracy of the computational model. Specifically, it must be verified that the computed results are not influenced by the grid size and/or the timestep used in simulations. To do so, a representative thermal runaway and fire propagation simulation is carried out. This simulation comprises two pallets with a 0.8 m distance between the two pallets. Dimensions of each pallet is assumed to be 0.184 m × 0.184 m × 0.069 m. Each pallet is assumed to contain one hundred 18650 NCA Li-ion cells at 25% SoC arranged in a 10 × 10 array with no cell-to-cell gap. The array of cells is wrapped in a 2 mm thick polyethylene sheet from all sides. The effect of all other pallet materials is ignored. Length, width and height of the storage room are assumed to be 3 m × 3 m × 5 m respectively. The trigger pallet is kept 0.6 m from the left boundary and 0.2 m from the front boundary, while the adjacent pallet is kept at the similar distance from front wall and 1.93 m from the right boundary of the simulation geometry. For computational simplicity and due to extremely small airgaps in the pallet, all cells in a pallet as well as the pallet material itself are homogenized and modeled as a single material in simulations. Based on past work, density and heat capacity of the material are taken to be 2280 kgm^{-3} and 715 $Jkg^{-1}K^{-1}$ respectively [13,47]. Thermal conductivity for the pallet material is 0.2 $Wm^{-1}K^{-1}$ in X and Y directions and 32 $Wm^{-1}K^{-1}$ in Z direction [13]. Standard thermal properties for polyethylene are assumed [48,49].

In order to examine the influence of the grid and timestep, simulations are carried out with a number of values of the maximum element size and maximum timestep. Keeping one of these parameters constant, the other parameter is reduced until the computed temperature field does not change significantly any more. Results are plotted in Fig. 2(a) and (b), in which, temperature at 0.5 m height above the trigger pallet is plotted as a function of time for multiple values of the maximum element size and maximum timestep, respectively. In these plots, the maximum timestep size is fixed at 0.0015 m for Fig. 2(a) and maximum element size is fixed at 0.01 s for Fig. 2(b). These results show that the temperature field changes somewhat when these parameters are changed, but becomes largely independent when the maximum element size is around 1.5 mm or lower, and when the maximum timestep is 10 ms or lower. Given the large physical size of the room and the long time period of interest, both of these are relatively small numbers, implying the considerable computational cost associated with these simulations. The very tight computational constraints needed to ensure grid- and timestep-independence is, however, not surprising, given the highly non-linear nature of combustion, turbulent flow as well as Arrhenius heat generation in this problem.

All further simulations discussed in this work are carried out with a maximum element size of 1.5 mm and a timestep of 10 ms.

3.2. Validation

In general, it is always desirable to validate a numerical computation framework, such as the one used in this work, by comparison with independent experimental measurements. Unfortunately, in the present case, there is a lack of sufficient experimental measurements on battery thermal runaway and fire propagation at the large length scales considered in this work. Therefore, a limited comparison of the present numerical framework with a previously reported experimental measurement on a single Li-ion cell [12] is carried out. Despite the smaller length scale involved in this comparison, this exercise helps establish the fundamental capability of the numerical computation framework to capture the key features of a thermal runaway event.

This comparison pertains to a thermal abuse measurement on a single 18650 cell in a fire calorimeter. Experimental measurements of surface temperature of a single 18650 NCA cathode type cell at 75% SoC were carried out during a fire test using cone calorimetry. External heating through 0.6 kW ceramic heater acts as the trigger to push cell into thermal runaway in a well-ventilated test chamber measuring 1.1 m $\times$ 1.1 m by 1.4 m. The conditions of this experiment are numerically simulated in the FDS computational framework, using the same governing equations as the rest of this work. All parameters, such as geometry and kinetics parameters of the cell are selected to match the conditions reported in the past experimental measurement [12]. Since Arrhenius kinetic parameters for single reaction thermal runaway model at 75% SoC are not available directly, these are approximated based on 50% and 100% SoC data. A comparison of measured surface temperature as a function of time with predictions from the numerical simulations is presented in Fig. 3, which shows reasonable agreement with the measured experimental data [12], both in terms of the time at which thermal runaway onset occurs, as well as the steep temperature rise and peak temperature attained during thermal runaway. Note that both experimental measurements and numerical simulations present some noise, mainly due to measurement and data acquisition noise in the experiment and the non-linear nature of the equations being solved in the simulation model. Nevertheless, the general agreement obtained in this comparison is encouraging.

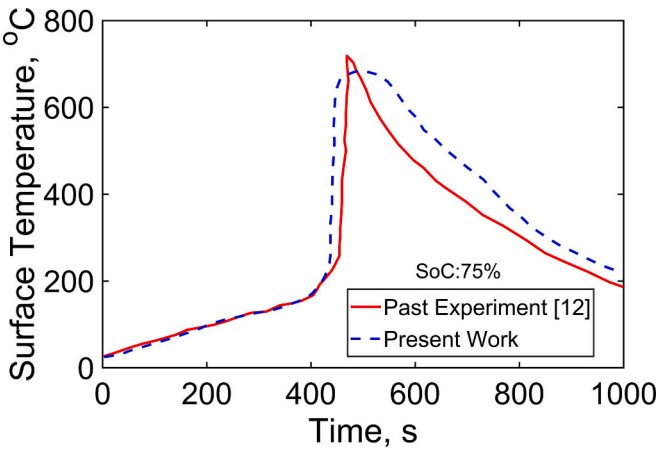

Fig. 3. Comparison of present work with past experimental data [12]: Temperature as a function of time for a single NCA 18650 cell at 75% SoC undergoing thermal runaway due to thermal abuse.

The comparison presented in Fig. 3 establishes the capability of the numerical simulation framework to capture the thermal runaway phenomenon, despite the limited nature of the validation carried out here, mainly due to lack of sufficient experimental data at the length scale of interest. Other papers in the past have also used FDS simulation framework to simulate fires originating from batteries and other sources [42–44], which further enhances the confidence in the present simulation framework.

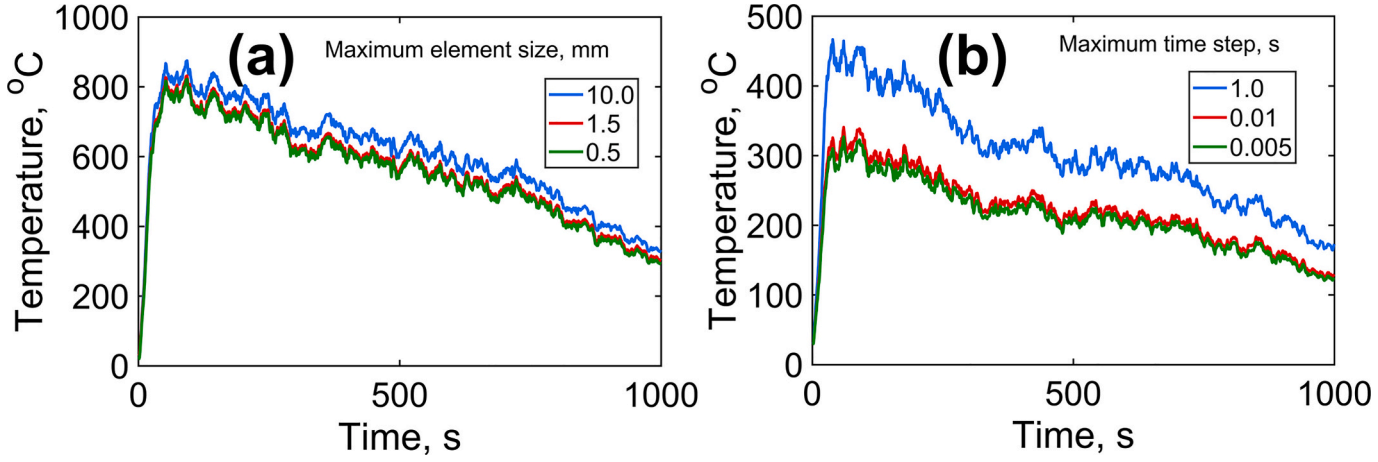

Fig. 2. Simulation results to establish mesh and time sensitivity: Temperature vs time plot at 0.5 m height from the trigger pallet at 25% SoC for (a) different element sizes and (b) for different maximum timestep bound in adaptive time stepping. Maximum timestep for (a) is 0.01 s and element size for (b) is 0.0015 m.

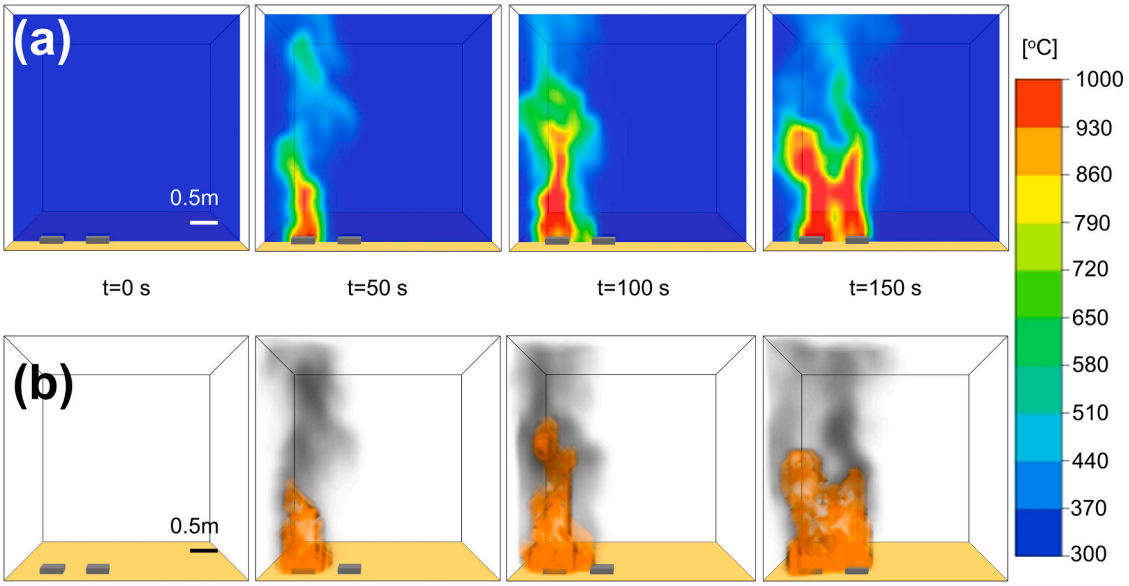

Fig. 4. (a) Temperature and (b) fire propagation color plots for the case of 0.6 m distance between trigger and adjacent pallets resulting in fire propagation. Cells in the trigger pallet are taken to be at 25% SoC.

3.3. *Typical temperature distribution*

Post-processing of simulation outputs are displayed using Smokeview software. Fig. 4 presents colorplots of the temperature field in a cross-section plane of the geometry at multiple times for a representative thermal runaway propagation scenario. For this simulation, the distance between trigger pallet and adjacent pallet is 0.6 m and the SoC is 25%. Single step abuse reaction model coupled with LES combustion model is implemented. Walls and ceiling of the simulation geometry are open to atmosphere. This mimics realistic fire propagation in a large storage facility where the concentration of oxygen is large compared to concentration of reactants. The colorplots in Fig. 4 show the trigger pallet (on the left) catch fire almost immediately. As time passes, heat transfer to the neighboring pallet causes its temperature to rise as well, eventually resulting in thermal runaway in the neighboring pallet too. In Fig. 4(b), total heat release rate (HRR) is plotted along with a soot density color plot to show fire propagation, based on the combustion of volatile gases released during thermal runaway as well as the pallet material. These plots clearly show combustion in the neighboring pallet occurring after some time.

The temperature data in colorplots in Fig. 4 can be plotted in order to provide a more comprehensive visualization of the temperature field over space and time. Fig. 5(a) plots temperature as a function of time at multiple locations above the trigger pallet for the set of conditions considered in Fig. 4. As expected, the highest temperature is encountered closest to the trigger pallet. Over time, temperature at each location first increases sharply due to rapid heat release during the thermal runaway process. After reaching a peak, the temperature then gradually comes down over a long period as the reactants are slowly consumed. A minor bump in the temperature curves around $t = 500$ s is associated with heat received from combustion of the neighboring pallet, which has a lag compared to combustion of the trigger pallet.

Fig. 5(b) plots temperature distributions above the trigger pallet at multiple times. The first curve shown, at $t = 200$ s, is close to the peak of fire in the trigger pallet, and, therefore, is the highest. Afterwards, the temperature field cools down as reactants get consumed. At each time, there is a gradual reduction in temperature with increasing vertical distance from the trigger pallet.

A similar plot of temperature as a function of time and space above the adjacent pallet is presented in Fig. 6. Fig. 6(a) and (b) plot

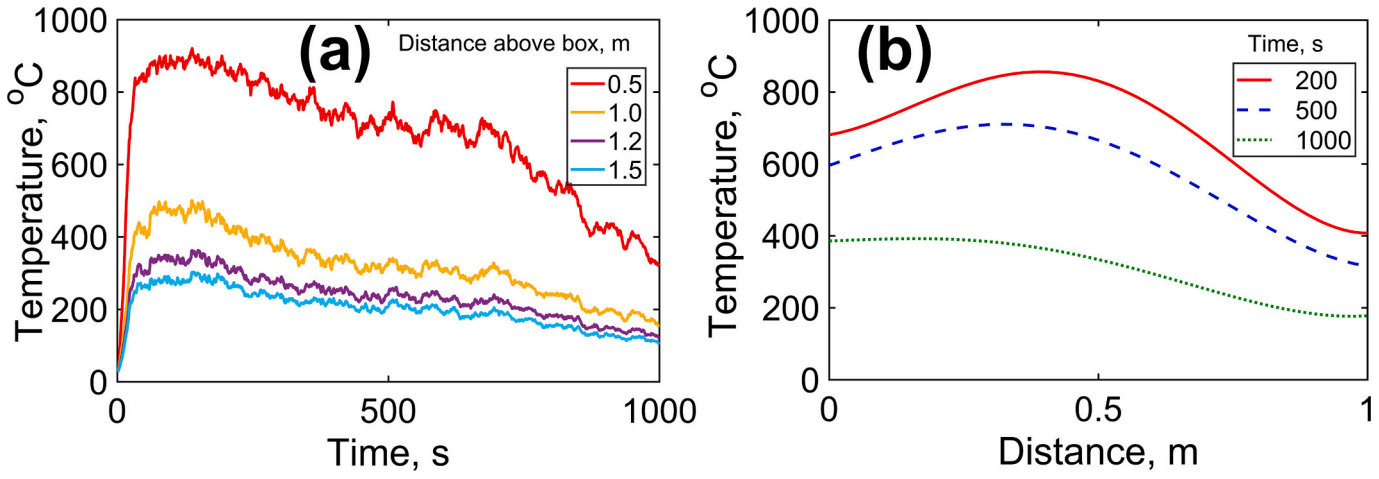

Fig. 5. Temperature plots above the trigger pallet: (a) Temperature as a function of time at different heights above the trigger pallet, and (b) temperature as a function of distance above the trigger pallet at multiple times. All conditions are the same as Fig. 4.

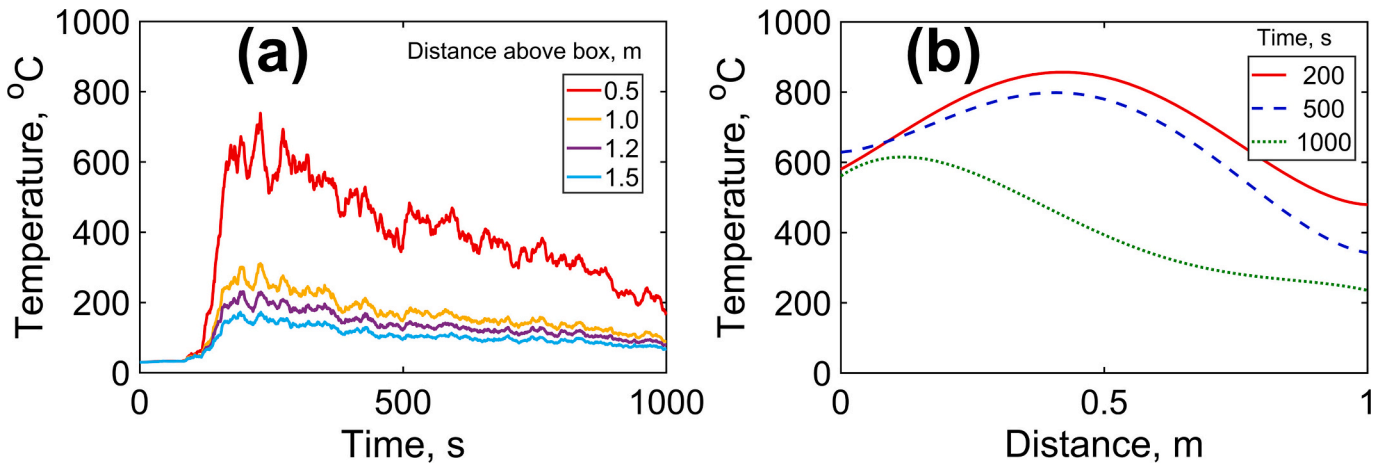

Fig. 6. Temperature plots above the adjacent pallet: (a) Temperature as a function of time at different heights above the adjacent pallet, and (b) temperature as a function of distance above the adjacent pallet at multiple times. All conditions are the same as Fig. 4.

temperature as a function of time at multiple locations above the adjacent pallet, and as a function of distance away from the adjacent pallet at multiple times, respectively. Fig. 6(a) shows a short period of no temperature rise above the adjacent pallet, followed by a large rise in temperature, and, finally, a gradual reduction. This short initial period corresponds to when the trigger pallet is on fire, but the fire has not yet spread to the adjacent pallet. Once the adjacent pallet catches fire, Fig. 6 (a) shows a sharp temperature rise, which lasts until the peak of combustion of the adjacent pallet. Afterwards, similar to the trigger pallet shown in Fig. 5(a), there is also a gradual reduction in the temperature field above the adjacent pallet. The spatial temperature distribution above the adjacent pallet at multiple times shown in Fig. 6(b) is somewhat more complicated than that above the trigger pallet because it is influenced by the time lag between fire in the trigger pallet and in the adjacent pallet. Each curve in Fig. 6(b) goes up, then down, which corresponds to the location of the flame. The temperature is the largest at the flame, and is lower both below and above the flame. As shown in these curves, the location of peak, i.e., the flame, reduces as time passes, which corresponds to the burnout of the flame once the reactants are consumed. It is interesting to note that the surface temperature of the adjacent pallet remains nearly constant. The small non-monotonicity of the surface temperature is explainable because the surface temperature first increases up to a certain time, and then reduces once the reactants begin to be consumed.

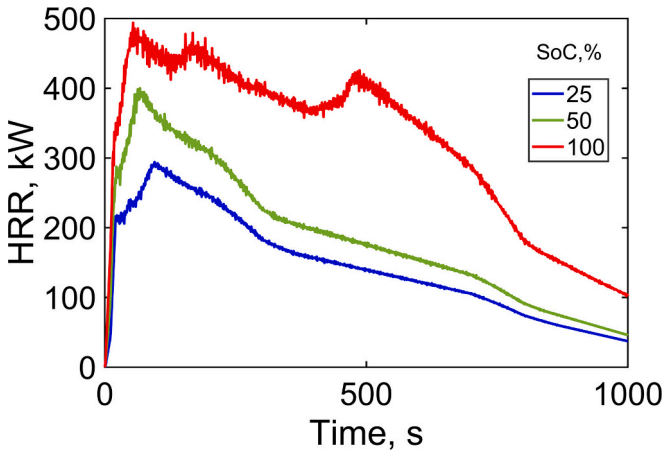

Fig. 7. Total heat release rate plot as a function of time for trigger pallet undergoing thermal runaway at different SoC.

3.4. Effect of SoC on onset

The SoC of a Li-ion cell plays a key role in determining its thermal runaway characteristics, and, therefore, is of much practical interest. The ideal SoC of cells during long-term storage or transportation has been widely debated [20,21]. Due to the practical importance of SoC, a number of simulations are carried out to characterize the role of SoC on the onset and propagation of fire from one pallet to another.

As described in Section 2.2.2, the effect of SoC is modeled in this work on the basis of previously reported values of activation energy and other kinetics parameters related to the thermal runaway reactions at different SoCs [11]. Data corresponding to Nickel Cobalt Aluminum Oxide (NCA) chemistry are used. Based on this, a number of simulations at three different SoCs (25%, 50% and 100%) are carried out. Fig. 7 presents plots of heat release rate as a function of time for a single pallet of cells undergoing thermal runaway for these values of SoC. As expected, the greater the SoC, the larger is the heat release rate, which is mainly due to greater energy content at higher SoC.

The greater heat release rate at higher SoC shown in Fig. 7 is expected to result in faster onset of thermal runaway and possibly greater temperature rise. This is confirmed by determining the temperature distribution in and around the trigger pallet for each SoC considered in Fig. 7. Fig. 8(a) presents temperature colorplots at $t = 400$ s for each SoC, whereas Fig. 8(b) plots temperature 1.0 m above the surface of the trigger pallet as a function for time for each SoC. As expected, thermal runaway is faster and more vigorous for the 100% SOC case, and there is propagation of thermal runaway to the adjacent pallet. The effect of SoC and pallet-to-pallet gap on thermal runaway propagation is analyzed in more detail in the next two sub-sections.

3.5. Effect of pallet-to-pallet gap

A key geometrical parameter of much practical relevance in this problem is the distance between adjacent pallets. Space is often limited in both storage and transportation of cells, and, therefore, in general, it is desirable to pack the battery pallets as close as possible to each other in order to increase the packing density. However, placing the pallets too close to each may increase heat transfer between adjacent cells, resulting in greater likelihood of propagation of thermal runaway from a trigger pallet to its neighbor.

In order to evaluate this interesting and important trade-off, temperature and fire color plots for a case with a large 0.8 m gap are plotted in Fig. 9 at 25% SoC. Compared to the baseline case of 0.6 m gap shown in Fig. 4, these colorplots clearly show that the larger gap results in the fire remaining isolated to only the trigger pallet. While the temperature

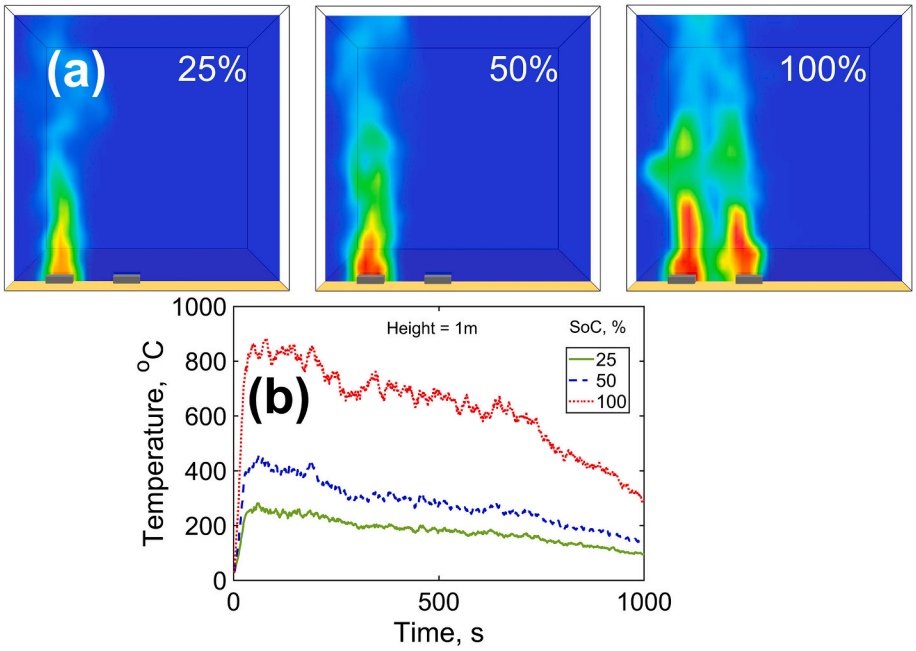

Fig. 8. (a) Temperature propagation color plots for the case of 0.8 m distance between trigger and adjacent pallet at different states of charge at 400 s and (b) Temperature as a function of SoC at 1.0 m height above trigger pallet.

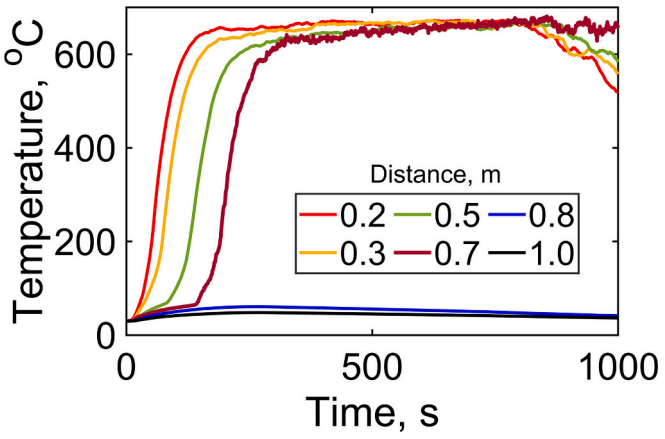

Fig. 9. Peak temperature at the top surface of the adjacent pallet as a function of time for different values of distance between trigger and adjacent pallets. Cells in the trigger pallet are taken to be at 25% SoC.

field above the trigger pallet shown in Fig. 9(a) is similar to the 0.6 m gap case, there is clearly no propagation of fire to the adjacent pallet as the pallet-to-pallet gap is too large for the fire to jump. This results in the impact of fire remaining somewhat isolated. This shows that the pallet-to-pallet gap plays a key role in determining the nature of fire in the storage facility. While on one hand, it may be desirable to reduce the pallet-to-pallet gap for more efficient packing, on the other hand, simulations presented here clearly show that a small pallet-to-pallet gap may risk the propagation of thermal runaway and fire from one pallet to the other.

In order to further illustrate the impact of pallet-to-pallet gap on thermal runaway and fire propagation, a number of simulations are carried out with different values of the gap between the trigger pallet and adjacent pallet, while keeping all other parameters fixed. Results are summarized in Fig. 10, where temperature at the surface of the adjacent pallet is plotted as a function of time for multiple values of the gap between the two pallets. It is found that for very small values of the gap, propagation of thermal runaway to the adjacent cell occurs very quickly, due to which, a rapid rise in temperature occurs, as shown in Fig. 10. As the value of the gap increases, propagation of thermal runaway still occurs, but with an increasing time delay. Eventually, at a cut-off value of the gap, there is a sudden change in the thermal runaway propagation characteristics of the system, so that for gaps beyond the cut-off value, there is no propagation of thermal runaway at all. There is still a minor increase in temperature in the adjacent pallet, but it is insufficient to sustain thermal runaway. For the parameter values considered here, Fig. 10 shows that the threshold value of the pallet-to-pallet gap is around 0.8 m.

Another interesting way to visualize the impact of pallet-to-pallet gap on thermal runaway propagation is to plot t_{Prop}, the time taken for propagation as a function of the pallet-to-pallet gap. This is plotted in Fig. 11, where the y axis represents the reciprocal of the time taken for propagation. This curve dips downwards as the gap increases, indicating a gradual increase in the time taken for propagation, until the cut-off value of the gap is reached. Beyond this cut-off, the curve abruptly drops to zero, indicating that there is no propagation of thermal runaway at all when the gap is greater than the cut-off value.

The existence of a sharp cut-off value of the gap has significant implications in the design of large-scale storage and transportation systems for Li-ion cells. The gap between pallets must clearly be kept above the cut-off gap because placing the pallets even slightly closer than dictated by the cut-off value results in a significant risk for thermal runaway propagation. If the current design of a storage facility has a pallet-to-pallet gap that is just below the threshold predicted by the simulations, it may be helpful to increase the gap slightly in order to go above the threshold and significantly improve safety with only an incremental impact on storage density.

Note that the cut-off value of the gap identified by Figs. 9 and 10 above is specific to the cell chemistry, pallet size, number of cells and other parameter values assumed in these simulations. For example, if the energy density of the pallet increases, the cut-off gap will likely grow as well due to greater heat released during thermal runaway. This will necessitate placing the pallets with greater gap.

3.6. *Effect of SoC on propagation*

While Section 3.4 investigated the impact of SoC mainly on the onset

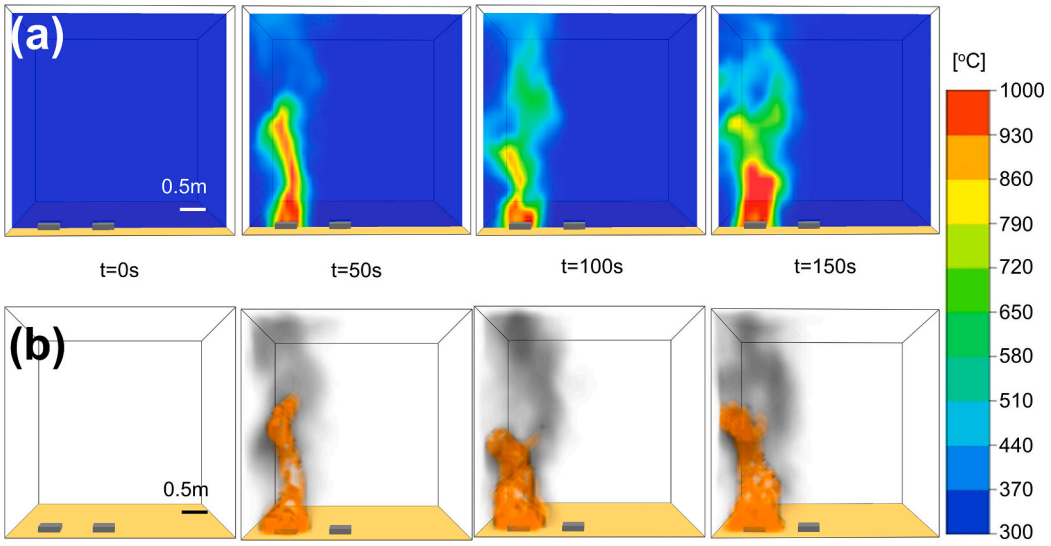

Fig. 10. (a) Temperature and (b) fire propagation color plots for the case of 0.8 m distance between trigger and adjacent pallets, resulting in no propagation of fire.

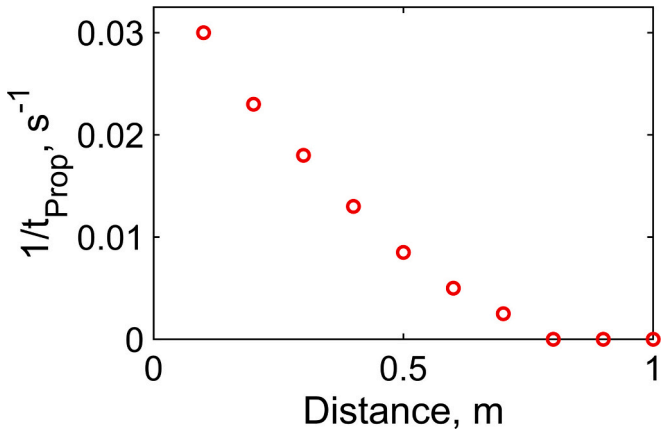

Fig. 11. Reciprocal of time taken for fire propagation to adjacent pallet as a function of distance between trigger pallet and adjacent pallet.

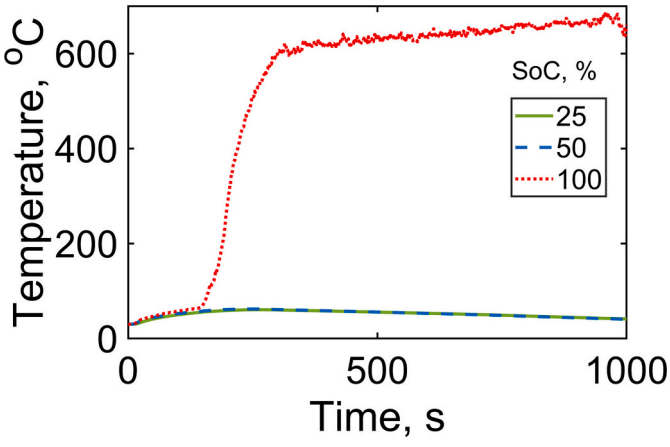

Fig. 12. Temperature at the surface of adjacent pallet as a function of time at three different SoCs for NCA cell chemistry.

of thermal runaway, it is also of interest to determine how the SoC of cells in the pallet affects the propagation of thermal runaway and fire from the trigger pallet to its neighbors. This is of much practical interest, since thermal runaway and fire limited to a single pallet, while not desirable, is a lot more acceptable than the other storage facility catching fire. Numerical simulations similar to those described in Section 3.5 are carried out at three different values of the SoC (25%, 50% and 100%). In each case, the pallet-to-pallet gap is kept fixed at 0.8 m. Fig. 12 presents plots of temperature on the surface of the adjacent pallet as a function of time for each SoC considered here. It is found that there is clearly propagation of thermal runaway and fire from the trigger pallet to adjacent pallet in the 100% SoC case. In contrast, the 50% and 25% SoC cases do not result in propagation, and while the trigger pallet undergoes thermal runaway, there is no spread of fire to the adjacent pallet. This is an important practical insight that may influence the design of SoC of cells under large-scale storage and/or transportation.

3.7. *Heat transfer mechanisms*

It is of interest to determine the relative importance of radiative and convective heat transfer mechanisms in the overall heat release rate from the trigger pallet. It is well known, for example, that as the

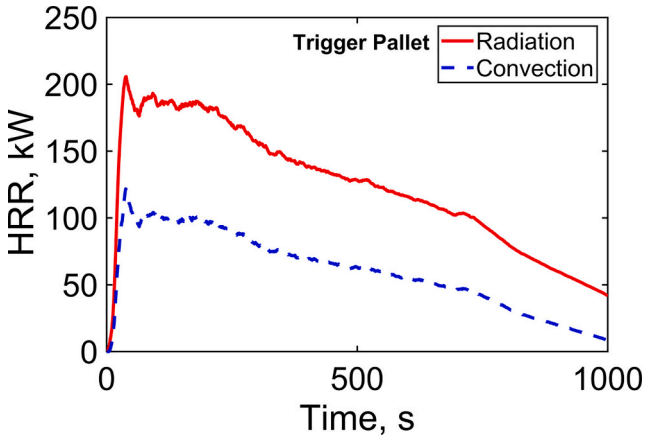

Fig. 13. Radiative and convective components of heat release rate from the trigger pallet as a function of time for 0.8 m pallet-to-pallet gap and 25% SoC.

temperature goes up, radiative heat transfer becomes more and more dominant. In order to investigate this for the present work, radiative and convective heat transfer components of the heat release rate from the pallet cells are computed for the baseline case of 0.8 mm pallet-to-pallet gap and 25% SoC. These data are plotted as function of time in Fig. 13. The plot indicates that radiative heat transfer is a dominant mechanism in heat release from the trigger pallet, particularly when the pallet temperature is high, around the time on onset of thermal runaway. As the temperature comes down during the cooling stage, both radiative and convective heat release rates drop. The decay in radiative heat release rate is steeper, as expected. These observations are all consistent with recent work on thermal runaway propagation in smaller battery packs [18].

4. Conclusions

Thermal safety of large battery storage and transportation systems requires a careful investigation of the multiple highly coupled processes that occur during thermal runaway. Given the cost and hazard associated with measurements, simulation models such as the one presented here may play a key role in guiding preliminary design and optimization. While much of past work in this direction has focused on thermal runaway at the scale of individual Li-ion cells, or a small pack of cells, the present work specifically addresses the important problem of battery safety during storage and transportation, when a very large number of cells may be packed densely in closely stored pallets. While simulation results are presented for a specific geometry and set of other parameters, the simulation framework can be easily scaled to model other scenarios, such as cells and pallets of other shapes and sizes. Other cell chemistries can also be modeled by appropriately changing the kinetics parameters of the decomposition reactions. Pallets also often contain other packaging materials such as wood, cardboard and plastics, which can also be easily modeled within the framework of these simulations.

Further, the vertical stacking of multiple pallets – not considered explicitly in the present work – may be of interest for future work. In such a scenario, the location of the trigger pallet within the vertical stack is likely to play a critical role in the propagation of thermal runaway. For example, hot combustion products rise up due to buoyancy, and, therefore, a trigger cell at the bottom of the stack may cause greater propagation than one at the top. Moreover, careful analysis and design of fire suppression systems such as sprinklers in the case of vertical stacking of pallets is needed. For example, the number of sprinklers and their locations relative to the trigger pallets likely plays a key role in determining the effectiveness of fire suppression, and, therefore, needs to be studied in detail. Finally, experimental validation of simulation results is also important and is identified as an important direction for future work.

Two key results from this work relate to the impact of SoC on thermal runaway propagation and the identification of a sharp threshold in terms of the pallet-to-pallet gap which governs whether fire propagation from one pallet to the other occurs or not. It is important for the design of large-scale storage and transportation of batteries to consider this trade-off between safety and density of battery storage. Based on this work, a detailed investigation is recommended to systematically understand fire prevention and suppression in large-scale battery storage and transportation scenarios.

CRediT authorship contribution statement

Dhananjay Mishra: Conceptualization, Methodology, Formal analysis, Investigation, Data curation, Visualization, Writing – original draft. **Raghavender Tummala:** Methodology, Writing – original draft. **Ankur Jain:** Conceptualization, Methodology, Formal analysis, Investigation, Data curation, Visualization, Project administration, Writing – original draft.

Declaration of competing interest

All authors hereby declare that they have no known competing financial interests or personal relationships that could have appeared to influence the work reported in this paper.

Data availability

Data will be made available on request.

References

[1] M.A. Hannan, M.M. Hoque, A. Hussain, Y. Yusof, P.J. Ker, State-of-the-art and energy management system of lithium-ion batteries in electric vehicle applications: issues and recommendations, IEEE Access. 6 (2018) 19362–19378.
[2] J.P. Fellner, G.J. Loeber, S.P. Vukson, C.A. Riepenhoff, Lithium-ion testing for spacecraft applications, J. Power Sources 119 (2003) 911–913.
[3] T. Chen, Y. Jin, H. Lv, et al., Applications of lithium-ion batteries in grid-scale energy storage systems, Trans. Tianjin Univ. 26 (2020) 208–217.
[4] K. Shah, V. Vishwakarma, A. Jain, Measurement of multiscale thermal transport phenomena in Li-ion cells: a review, J. Electrochem. Energy Convers. Storage 13 (2016).
[5] A.W. Golubkov, D. Fuchs, J. Wagner, et al., Thermal-runaway experiments on consumer Li-ion batteries with metal-oxide and olivin-type cathodes, RSC Adv. 4 (2014) 3633–3642.
[6] K. Shah, D. Chalise, A. Jain, Experimental and theoretical analysis of a method to predict thermal runaway in Li-ion cells, J. Power Sources 330 (2016) 167–174.
[7] P. Jindal, J. Bhattacharya, Review—understanding the thermal runaway behavior of Li-ion batteries through experimental techniques, J. Electrochem. Soc. 166 (2019) A2165–A2193.
[8] X. Feng, S. Zheng, D. Ren, et al., Investigating the thermal runaway mechanisms of lithium-ion batteries based on thermal analysis database, Appl. Energy 246 (2019) 53–64.
[9] G.H. Kim, A. Pesaran, R. Spotnitz, A three-dimensional thermal abuse model for lithium-ion cells, J. Power Sources 170 (2007) 476–489.
[10] I. Esho, K. Shah, A. Jain, Measurements and modeling to determine the critical temperature for preventing thermal runaway in Li-ion cells, Appl. Therm. Eng. 145 (2018) 287–294.
[11] J. Kim, A. Mallarapu, D.P. Finegan, S. Santhanagopalan, Modeling cell venting and gas-phase reactions in 18650 lithium ion batteries during thermal runaway, J. Power Sources 489 (2021), 229496.
[12] P.V. Chombo, Y. Laoonual, Prediction of the onset of thermal runaway and its thermal hazards in 18650 lithium-ion battery abused by external heating, Fire Saf. J. 129 (2022), 103560.
[13] S.J. Drake, D.A. Wetz, J.K. Ostanek, S.P. Miller, J.M. Heinzel, A. Jain, Measurement of anisotropic thermophysical properties of cylindrical Li-ion cells, J. Power Sources 252 (2014) 298–304.
[14] W. Allafi, C. Zhang, K. Uddin, et al., A lumped thermal model of lithium-ion battery cells considering radiative heat transfer, Appl. Therm. Eng. 143 (2018) 472–481.
[15] P.T. Coman, S. Rayman, R.E. White, A lumped model of venting during thermal runaway in a cylindrical lithium cobalt oxide lithium-ion cell, J. Power Sources 307 (2016) 56–62.
[16] A. Melcher, C. Ziebert, M. Rohde, H.J. Seifert, Modeling and simulation of the thermal runaway behavior of cylindrical Li-ion cells-computing of critical parameters, Energies 9 (2016) 1–19.
[17] D. Ren, X. Feng, L. Liu, et al., Investigating the relationship between internal short circuit and thermal runaway of lithium-ion batteries under thermal abuse condition, Energy Storage Mater. 34 (2021) 563–573.
[18] D. Mishra, A. Jain, Multi-mode heat transfer simulations of the onset and propagation of thermal runaway in a pack of cylindrical Li-ion cells, J. Electrochem. Soc. 168 (2021), 020504.
[19] M. Chen, D. Ouyang, J. Weng, J. Liu, J. Wang, Environmental pressure effects on thermal runaway and fire behaviors of lithium-ion battery with different cathodes and state of charge, Process. Saf. Environ. Prot. 130 (2019) 250–256.
[20] Q. Zhang, J. Niu, Z. Zhao, Q. Wang, Research on the effect of thermal runaway gas components and explosion limits of lithium-ion batteries under different charge states, J. Energy Storage 45 (2022), 103759.
[21] J. Fang, J. Cai, X. He, Experimental study on the vertical thermal runaway propagation in cylindrical Lithium-ion batteries: effects of spacing and state of charge, Appl. Therm. Eng. 197 (2021), 117399.
[22] D. Mishra, K. Shah, A. Jain, Investigation of the impact of radiative shielding by internal partitions walls on propagation of thermal runaway in a matrix of cylindrical Li-ion cells, J. Electrochem. Soc. 168 (2021), 120507.
[23] D. Mishra, K. Shah, A. Jain, Investigation of the impact of flow of vented gas on propagation of thermal runaway in a Li-ion battery pack, J. Electrochem. Soc. 168 (2021), 060555.
[24] D. Mishra, P. Zhao, A. Jain, Thermal runaway propagation in Li-ion battery packs due to combustion of vent gases, J. Electrochem. Soc. 169 (2022), 100520.
[25] C. Yuan, Q. Wang, Y. Wang, Y. Zhao, Inhibition effect of different interstitial materials on thermal runaway propagation in the cylindrical lithium-ion battery module, Appl. Therm. Eng. 153 (2019) 39–50.

[26] F.A. Mier, Fluid Dynamics of Lithium Ion Battery Venting Failures, Ph.D. Dissertation, New Mexico Institute of Mining and Technology, 2020.
[27] M. Parhizi, A. Jain, G. Kilaz, J.K. Ostanek, Accelerating the numerical solution of thermal runaway in Li-ion batteries, J. Power Sources 538 (2022), 231531.
[28] Y. Chen, Y. Kang, Y. Zhao, et al., A review of lithium-ion battery safety concerns: the issues, strategies, and testing standards, J. Energy Chem. 59 (2021) 83–99.
[29] P. Ping, Q.S. Wang, P.F. Huang, et al., Study of the fire behavior of high-energy lithium-ion batteries with full-scale burning test, J. Power Sources 285 (2015) 80–89.
[30] T. Dagger, B.R. Rad, F.M. Schappacher, M. Winter, Comparative performance evaluation of flame retardant additives for lithium ion batteries–I. Safety, chemical and electrochemical stabilities, Energy Technol. 6 (2018) 2011–2022.
[31] X. Zhang, Q. Sun, C. Zhen, et al., Recent progress in flame-retardant separators for safe lithium-ion batteries, Energy Storage Mater. 37 (2021) 628–647.
[32] L.B. Diaz, X. He, Z. Hu, F. Restuccia, M. Marinescu, J.V. Barreras, Y. Patel, G. Offer, G. Rein, Review—Meta-Review of Fire Safety of Lithium-Ion Batteries: Industry Challenges and Research Contributions, J. Electrochem. Soc. 167 (2020), 090559.
[33] J. Xie, J. Li, J. Wang, J. Jiang, Fire protection design of a lithium-ion battery warehouse based on numerical simulation results, J. Loss Prev. Process Ind. 80 (2022), 104885.
[34] A.L. Sullivan, Wildland surface fire spread modelling, 1990–2007. 3: simulation and mathematical analogue models, Int. J. Wildl. Fire 18 (2009) 387–403.
[35] V.V. Ganesan, A. Jain, Computationally-efficient thermal simulations of large Li-ion battery packs using submodeling technique, Int. J. Heat Mass Transf. 165 (2021), 120616.
[36] P.T. Coman, E.C. Darcy, B. Strangways, R.E. White, A reduced-order lumped model for Li-ion battery packs during operation, J. Electrochem. Soc. 168 (2021), 100525.
[37] G.G. Eshetu, S. Grugeon, S. Laruelle, et al., In-depth safety-focused analysis of solvents used in electrolytes for large scale lithium ion batteries, Phys. Chem. Chem. Phys. 15 (2013) 9145–9155.
[38] A.W. Golubkov, S. Scheikl, R. Planteu, et al., Thermal runaway of commercial 18650 Li-ion batteries with LFP and NCA cathodes - impact of state of charge and overcharge, RSC Adv. 5 (2015) 57171–57186.
[39] C.G. Speziale, Turbulence modeling for time-dependent RANS and VLES: a review, AIAA J. 36 (1998) 173–184.
[40] C.K. Westbrook, F.L. Dryer, Simplified reaction mechanisms for the oxidation of hydrocarbon fuels in flames, Combust. Sci. Technol. 27 (1–2) (1981) 31–43.
[41] K.B. McGrattan, G.P. Forney, Fire Dynamics Simulator: User's Manual, National Institute of Standards and Technology Report No. NISTIR-6469, 2000.
[42] D. Brzezinska, P. Bryant, Performance-based analysis in evaluation of safety in car parks under electric vehicle fire conditions, Energies 15 (2) (2022).
[43] D. Brzezińska, Ventilation system influence on hydrogen explosion hazards in industrial lead-acid battery rooms, Energies 11 (8) (2018) 1–11.
[44] A. Yip, J.B. Haelssig, M.J. Pegg, Simulating fire dynamics in multicomponent pool fires, Fire Saf. J. 125 (June) (2021), 103402.
[45] T.F. Russell, Stability analysis and switching criteria for adaptive implicit methods based on the CFL condition, in: SPE Symposium on Reservoir Simulation, OnePetro, 1989.
[46] P.E.O. Buelow, S. Venkateswaran, C.L. Merkle, Stability and convergence analysis of implicit upwind schemes, Comput. Fluids 30 (7–8) (2001) 961–988.
[47] M. Parhizi, M.B. Ahmed, A. Jain, Determination of the core temperature of a Li-ion cell during thermal runaway, J. Power Sources 370 (2017) 27–35.
[48] J. Fujino, T. Honda, Measurement of the specific heat of plastic waste/fly ash composite material using differential scanning calorimetry, Int. J. Thermophys. 30 (3) (2009) 976–986.
[49] A. Yamanaka, T. Takao, Thermal conductivity of high-strength polyethylene fiber and applications for cryogenic use, Int. Sch. Res. Not. 2011 (2011), 718761, https://doi.org/10.5402/2011/718761.